





Article

On the Influence of Unexpected Earthquake Severity and Dampers Placement on Isolated Structures Subjected to Pounding Using the Modified Endurance Time Method

Ali Majdi ¹, Ataallah Sadeghi-Movahhed ², Mohammadreza Mashayekhi ³, Saeid Zardari ⁴,
Omrane Benjeddou ⁵ and Dario De Domenico ^{6,*}

¹ Department of Buildings and Construction Techniques Engineering, College of Engineering, Al-Mustaqbal University, Hillah 51001, Babylon, Iraq; alimajdi@uomus.edu.iq

² Department of Civil Engineering, Shabestar Branch, Islamic Azad University, Shabestar 5381637181, Iran; a.sadeghimovahhed@gmail.com

³ Department of Civil Engineering, K.N. Toosi University of Technology, Tehran 1996715433, Iran; m.mashayekhi@kntu.ac.ir

⁴ Department of Civil Engineering, Istanbul Okan University, Istanbul 34959, Turkey; saeid.zardari@okan.edu.tr

⁵ Department of Civil Engineering, College of Engineering, Prince Sattam bin Abdulaziz University, Alkharj 11942, Saudi Arabia; benjeddou.omrane@gmail.com

⁶ Department of Engineering, University of Messina, 98166 Messina, Italy

* Correspondence: dario.dedomenico@unime.it



Citation: Majdi, A.;

Sadeghi-Movahhed, A.; Mashayekhi, M.; Zardari, S.; Benjeddou, O.; De Domenico, D. On the Influence of Unexpected Earthquake Severity and Dampers Placement on Isolated Structures Subjected to Pounding Using the Modified Endurance Time Method. *Buildings* **2023**, *13*, 1278. <https://doi.org/10.3390/buildings13051278>

Academic Editor: Hugo Rodrigues

Received: 25 April 2023

Revised: 7 May 2023

Accepted: 11 May 2023

Published: 14 May 2023



Copyright: © 2023 by the authors. Licensee MDPI, Basel, Switzerland. This article is an open access article distributed under the terms and conditions of the Creative Commons Attribution (CC BY) license (<https://creativecommons.org/licenses/by/4.0/>).

Abstract: The aim of this study is to investigate the performance of isolated structures by considering the possibility of impact under severe earthquakes. In the design of isolated structures, the required displacement capacity is determined based on the considered earthquake hazard level. However, there is a possibility of an impact caused by moat walls or adjacent structures under severe earthquakes. Dampers are used in this study to improve the performance of structural and nonstructural components. In this regard, three isolated structures (6, 9, and 12 stories) equipped with Triple Friction Pendulum Isolator (TFPI) are designed under earthquake hazard levels of BSE-1 with return periods of 475 years. Based on the different positions of these three structures relative to each other, four scenarios are defined to investigate the effect of impact. Modified endurance time (MET) method, as a cost-efficient nonlinear time history analysis method, is employed for structural evaluation under variable earthquake hazard levels. The placement of dampers is also taken into account in evaluating the effect of dampers. Therefore, the structures have been retrofitted once by adding damping and stiffness devices (ADAS) on the stories and once by adding fluid viscous dampers (FVD) at the isolated level. Results indicate that structures might collapse under earthquake hazard levels of BSE-2 with return periods of 2475 years. This matter is influenced by the adjacency of two isolated structures next to each other, and the severity of this fact depends on the height of the structures and the displacement capacity of the isolators so that the tall, isolated structures have decreased the performance of the adjacent shorter isolated structure. Moreover, the placement of dampers has a significant influence on the performance of structural and nonstructural components, depending on the reason for the impact.

Keywords: base isolation; endurance time analysis; impact; adding damping and stiffness devices (ADAS); fluid viscous damper (FVD); seismic resilience

1. Introduction

Seismic isolators are developing rapidly as one of the practical systems against earthquakes [1–3]. Various evaluations have been performed on these systems [4–6]. Pounding is one of the phenomena that researchers try to prevent when designing of isolated structures. Komodromos et al. [7] found that pounding in isolated structures causes the excitation

of higher modes. The pounding phenomenon also causes acceleration to become critical in the lower stories of the structure. In an experimental research work, Masroor and Mosqueda [8] concluded that the maximum drift increases uniformly in all stories of the isolated structure under pounding with lower impact velocities. The acceleration also increases non-uniformly in the story under the pounding phenomenon.

According to Masroor and Mosqueda [9], when there is no impact, an isolated structure with an ordinary concentric braced frame (OCBF) performs better than one with an intermediate moment frame (IMF). However, when the impact effect at a calculated distance, according to ASCE7-05 [10], is considered, the probability of collapse is lower for the IMF than the OCBF. Matsagar and Jangid [11] observed that the acceleration of higher stories increases in pounding with a stiffer adjacent structure. Moreover, the acceleration of the isolated structure is lower than the fixed base structure under impact. Pant and Wijeyewickrema [12] showed that the behavior of an isolated structure under impact with a moat wall on both sides or one side of the structure is more critical than the impact between a fixed base structure on one side and a moat wall on the other side. A great ductility demand is imposed during impact on isolated structures with a stiff superstructure [13]. Therefore, the damage starts from the superstructure, and more isolator displacement capacity is needed.

Increasing the yield strength in isolated structures with flexible superstructure has been concluded to be more advantageous than the stiff superstructure. Moreover, increasing the post-yield stiffness of the superstructure is more effective for isolated structures with a stiff superstructure [14]. Sadeghi Movahhed et al. [15] investigated the effect of increasing the superstructure stiffness and the triple friction pendulum isolator (TFPI) damping on the reduction in the pounding effects. The results showed that the mentioned methods are ineffective in reducing the vulnerability of nonstructural components. Rayegani and Nouri [16] used a magnetorheological damper on the isolated level along with a high-damping rubber isolator using a modified fuzzy-based controller to control the pounding effect in a four-story structure with a moat wall. They stated that the mentioned control system is suitable for achieving an acceptable collapse probability in isolated structures without sufficient displacement capacity. Rawlinson et al. [17] showed that the performance of a gap damper is desirable to reduce pounding in an isolated structure. Zargar et al. [18] found that using a viscous damper as a gap damper is more effective than a damper with just a hysteretic behavior. A gap damper has been found to be more effective against unidirectional motions or motions with a strong unidirectional component [19]. Investigation of the effect of using a viscoelastic damper between adjacent isolated structures floors showed that the viscoelastic damper significantly reduces the maximum displacement and pounding effects [20]. A hybrid control strategy including base isolation and inline dampers has been reported to have better performance than semi-active control systems to deal with the impact of the adjacent structures [21]. The use of rubber bumpers has been introduced as an effective method to reduce peak impact force in isolated structures [22]. Zhou and Chen [23] conducted a shaking table test on an isolated concrete structure and found that a supplementary viscous damper installed at the isolation level can decrease seismic response during relatively low-intensity earthquakes. However, for higher-intensity earthquakes, the same viscous damper can have a negative impact on the response of the superstructure. Furthermore, Chen and Wu [24] demonstrated that connecting adjacent buildings with dampers to avoid pounding is more effective in mitigating seismic impact when the two ends of the dampers are connected on different levels.

As can be seen, the pounding phenomenon is a fundamental problem in the design of isolated structures. However, this becomes more critical when the isolated structure is exposed to an earthquake more severe than the predicted earthquake in the design step. For example, it is stated in the ASCE7-16 [25] that seismic isolators must be designed for earthquake hazard levels of BSE-2 with return periods of 2475 years. However, in the ASCE7-10 [26], it was allowed that isolated structures can be designed for earthquake hazard levels of BSE-1 with return periods of 475 years. Hence, the behavior of the designed

structure for the BSE-1 hazard level under the BSE-2 hazard level is unknown. Increasing the earthquake intensity leads to an increase in the displacement of the isolator. Therefore, there is a possibility of the pounding phenomenon in the mentioned conditions. However, Kitayama and Constantinou [27] showed that there is still a possibility of collapse by providing the minimum displacement requirement according to ASCE7-16 [25] for isolated structures under the BSE-2 hazard level. Therefore, there is also the possibility of failure in structures designed according to ASCE7-10 [26] under the BSE-2 hazard level. In most past studies (mentioned above), the vulnerability of isolated structures due to the change in the earthquake hazard level has not been investigated, while one of the reasons for the impact of the isolated structure is that the applied earthquake intensity is higher than the earthquake hazard level considered in the design step. Therefore, this paper investigates the vulnerability of the existing three isolated structures with different heights under the BSE-2 hazard level, which are designed based on ASCE 7-10 [26]. The displacement capacity of the isolator is considered equal to the required capacity for the BSE-1 hazard level. Hence, the structures are subjected to pounding. Using a damper is one of the effective methods to increase the performance of structures [28,29]. The damper placement can be on the floors or at the isolated level of structures. However, the damper position can be effective on the seismic results of isolated structures under impact. To this end, the effect of dampers placement to reduce the effects of pounding is also investigated. The Section 2 introduces the modified endurance time (MET) method, which is used to evaluate structures. In Section 3, we present the structures and scenarios under consideration, including the frame design specifications, the manner in which pounding occurs, and the assumptions made when modeling this phenomenon. Section 4 outlines the process of designing, modeling, and installing passive control systems in structures, which involves the use of TFPI, fluid viscous damper (FVD), and adding damping and stiffness device (ADAS). Section 5 examines four scenarios in which pounding occurs, such as collisions between the structure and the moat wall or adjacent structures. Finally, Section 6 summarizes the research conducted and explains the results obtained.

2. Modified Endurance Time Method

The Endurance Time (ET) method was developed by Estekanchi et al. [30] as a form of dynamic analysis. It involves applying a set of pre-designed artificial accelerograms, known as endurance time excitation functions (ETEFs), regarding a structure. ETEFs are ramp-like, and their amplitude increases over time [31]. ETEFs are produced using optimization techniques and the concept of response spectra [32]. Five generations of ETEFs have been generated, which have different characteristics. In the first generation of ETEFs, the theory of random vibrations is used. The purpose of generating the first-generation ETEFs was to introduce the concept of the ET method. Second-generation ETEFs were produced for the analysis of structures. The linear response spectrum compatibility was used to generate these records. The optimization process was used to solve the equations and generate these ETEFs [33]. The matching of nonlinear responses was also considered in the production of third-generation ETEFs. A series of research projects regarding the compatibility of the duration of ET records and real recorded ground motions concluded that although there is acceptable compatibility between ETEFs and ground motions, it is recommended to consider the duration compatibility in the production of records [34,35]. In this regard, the fourth generation of ETEFs was produced in terms of duration compatibility [36]. Hysteretic energy compatibility [37] was investigated for the more accurate ETEFs. It was demonstrated that better ETEFs would be produced if hysteretic energy was included in the production process [38]. Therefore, the fifth-generation ETEF was introduced. In the present study, fifth-generation ETEFs are employed, which are introduced as the ETA40kd series. The ETA40kd series is generated so that they would be compatible with 22 far-fault records of FEMA-P695 [39]. This series includes ETA40kdx01-03, ETAkdy01-03, and ETA40dz01-03. Indeed, there are three ETEFs for each direction. The duration of ETEFs is 40.95 s. Figure 1 shows the accelerograms of ETA40kdx01-03. Moreover, acceptable

consistency for the average response spectrum of ETA40kdx01-03 with target acceleration spectra at 5, 10, and 15 s are represented in Figure 2. In some cases, the required time for ETEFs (target time) to produce the intensity level equal to the desired earthquake hazard level is longer than the length of ETEFs. This matter is more likely in isolated structures due to their long period. This study utilizes the MET method developed by Sadeghi Movahhed et al. [40] to solve this problem. In the MET method, the combination of different scale factors is included in the seismic response assessment. Adding a scale factor to ETEFs leads to a reduction in the target time.

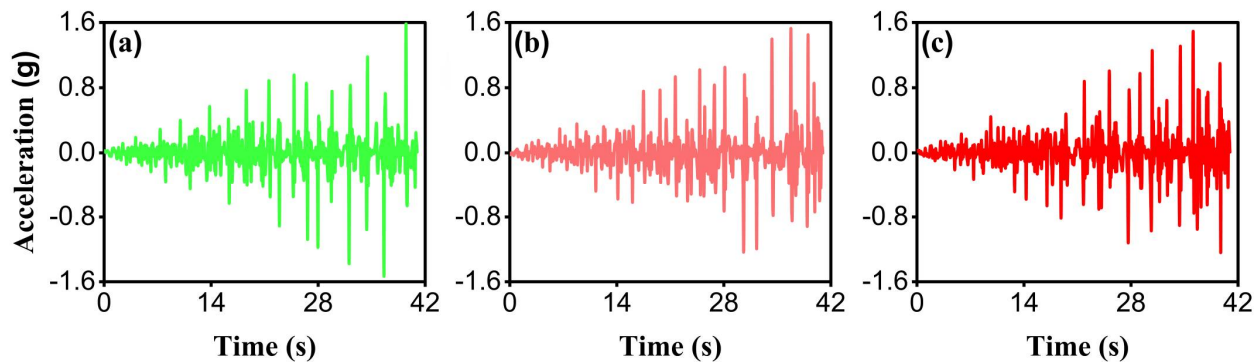


Figure 1. Excitation functions of ETA40kdx01-03: (a) ETA40kdx01; (b) ETA40kdx02; (c) ETA40kdx03.

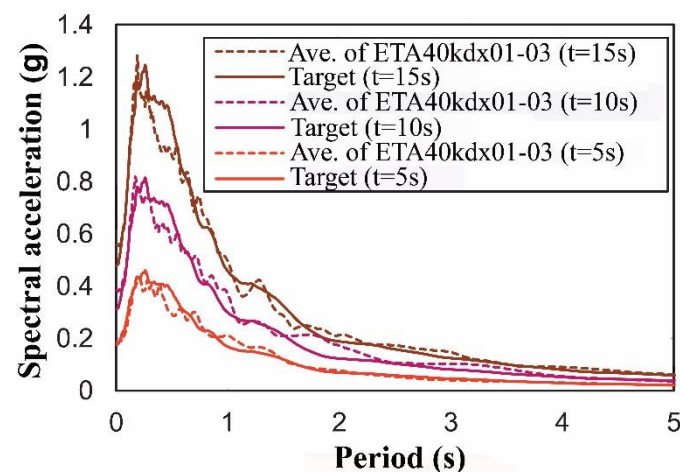


Figure 2. Comparison between the average response spectrum of ETA40kdx01-03 and target acceleration spectra at 5, 10, and 15 s.

3. Numerical Models

In this study, three isolated steel frames (6, 9 and 12 stories) with TFPI are considered (Figure 3). IMF is used as the lateral force-resisting system of the superstructure. Each frame has 3 bays with a length of 5 m, and the height of each story is 3.2 m. These frames are located on soil type C, whose risk-targeted for the BSE-1 hazard level is equal to $S_{DS} = 1$ and $S_{D1} = 0.4$. ASCE 7-10 [26], AISC 360 [41], and AISC 341 [42] have been used to design frames. The specifications of the superstructure steel materials including the yielding stress, the ultimate stress and the modulus of elasticity are $F_y = 23.5 \text{ kN/cm}^2$, $F_u = 39.22 \text{ kN/cm}^2$, $E_s = 20,000 \text{ kN/cm}^2$, respectively. The dead load on all beams is 45 kN/m and the live load for stories and roof beams is 15 kN/m and 9 kN/m, respectively. Since the structure is affected by the impact, the nonlinear behavior of the materials is considered by assigning flexural plastic hinges at both ends of beams and axial–flexural interaction hinges at both ends of columns according to ASCE41-17 [43]. In SAP2000 software [44], the plastic hinges for columns and beams are defined as P-M3 and M3, respectively. These hinges correspond to performance levels of immediate occupancy (IO), life safety (LS), and collapse prevention

(CP). To account for the effect of strain stiffness, the slope of the region (C-D) shown in Figure 4 is set to 3% of the slope of the elastic portion.

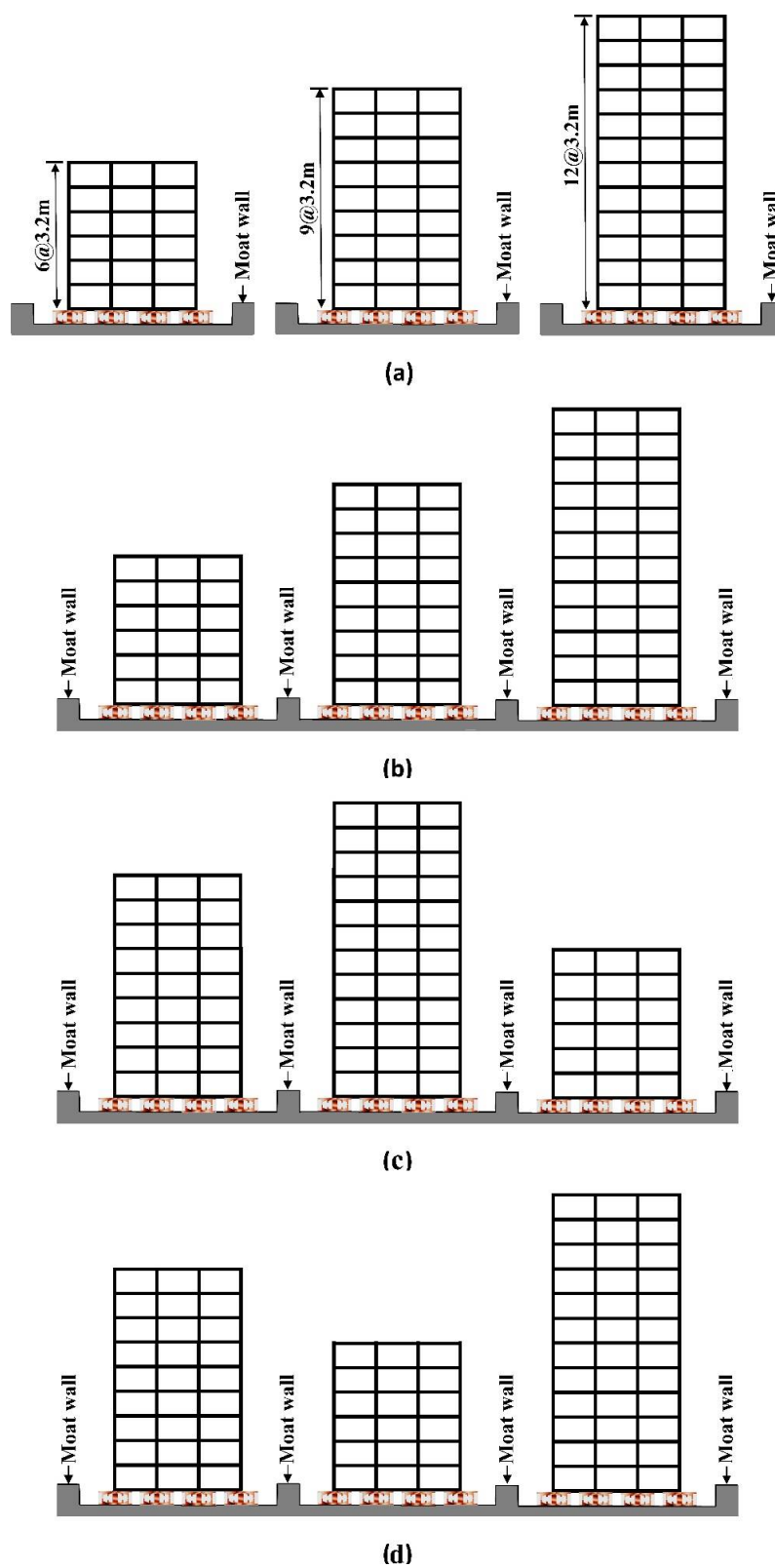


Figure 3. Schematic view of the isolated frames: (a) Scenario 1; (b) Scenario 2; (c) Scenario 3; (d) Scenario 4.

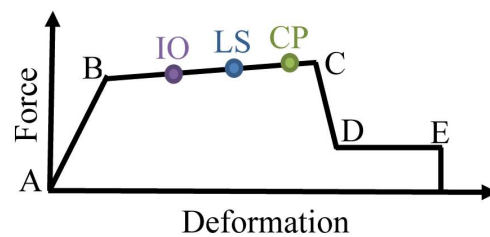


Figure 4. Force-deformation curve of steel sections.

The equivalent lateral force (ELF) method is used to design frames in SAP2000 software [44]. The periods of structures without TFPI (T_S) are 1.1 s, 1.5 s, and 1.89 s for 6, 9, and 12-story structures, respectively. The periods of isolated structures (T_D) are considered 3.3 s for the 6- and 9-story frame and 4.4 s for the 12-story frame. The T_D/T_S ratio is selected according to the results of the research by Sadeghi Movahhed et al. [45]. The designed sections for the superstructures are provided in Table 1.

Table 1. Sections of the superstructure.

Floor Level	Column			Beam		
12				W16×50		
11	W12×35			W18×50		
10	W12×58			W18×55		
9	W12×72			W18×65	W18×50	
8	W12×72	W12×35		W18×71	W18×50	
7	W12×87	W12×45		W18×76	W18×60	
6	W12×96	W12×58		W18×86	W18×65	W16×50
5	W12×106	W12×72	W12×35	W18×86	W18×71	W16×50
4	W12×120	W12×79	W12×45	W18×86	W18×76	W16×50
3	W12×136	W12×96	W12×65	W18×86	W18×76	W16×57
2	W12×136	W12×106	W12×65	W18×86	W18×76	W16×57
1	W12×152	W12×120	W12×79	W18×86	W18×76	W16×57
0 (Isolated level)	W12×170	W12×136	W12×79	W21×201	W21×201	W21×201

Four scenarios have been considered based on the placement position of structures. In the first scenario, only the moat wall is located around the structures, and in the second to fourth scenarios, in addition to the moat wall, isolated structures are placed next to each other (Figure 3). The displacement capacity of the isolated structure is determined based on the minimum required displacement of the isolator (D_D) for the BSE-1 hazard level. However, the structure will be subjected to the BSE-2 hazard level and as a result, pounding will occur. There is only a collision between the moat wall and the structure in scenario 1. In scenarios 2 to 4, in addition to the collision of the structure with the moat wall, adjacent structures also collide with each other. D_D for 6, 9, and 12-story structures is 28.5 cm, 26.8 cm, and 30 cm, respectively. These values are obtained from the MET method, which according to ASCE7-10 [26] are more than 90% of the obtained results from the ELF method. The gap element is used in SAP2000 software [44] to model the moat wall. Indeed, the impact phenomenon is simulated as a linear behavior. An adequate estimate of the pounding effect can be obtained by employing a linear elastic spring. However, the oscillatory behavior may be present in the linear elastic model [46]. The backfill soil–structure interaction is neglected. Pant and Wijeyewickrema’s method [12] is used in the present study, in which the value of impact stiffness is equal to the axial stiffness of the building slab. It should be noticed that the impact stiffness value for a moat wall is still under research [14].

4. Design and Modeling of Passive Control Systems

4.1. TFPI

The TFPI isolator (Figure 5a) is the developed model of the single friction pendulum isolator that was introduced by Fenz and Constantinou [47,48]. Fenz and Constantinou [49] presented the series method to model the TFPI isolation in SAP2000 software [44], in which the TFPI is simulated by modeling three single friction pendulum isolators in series. In this research, this method is used to model TFPI. Figure 6 shows the TFPI design steps [50]. The force-displacement relationship considered in the design process of TFPI is shown in Figure 5b, while the full hysteresis loop is shown in Figure 5c. Additionally, the obtained specifications of TFPI are demonstrated in Table 2.

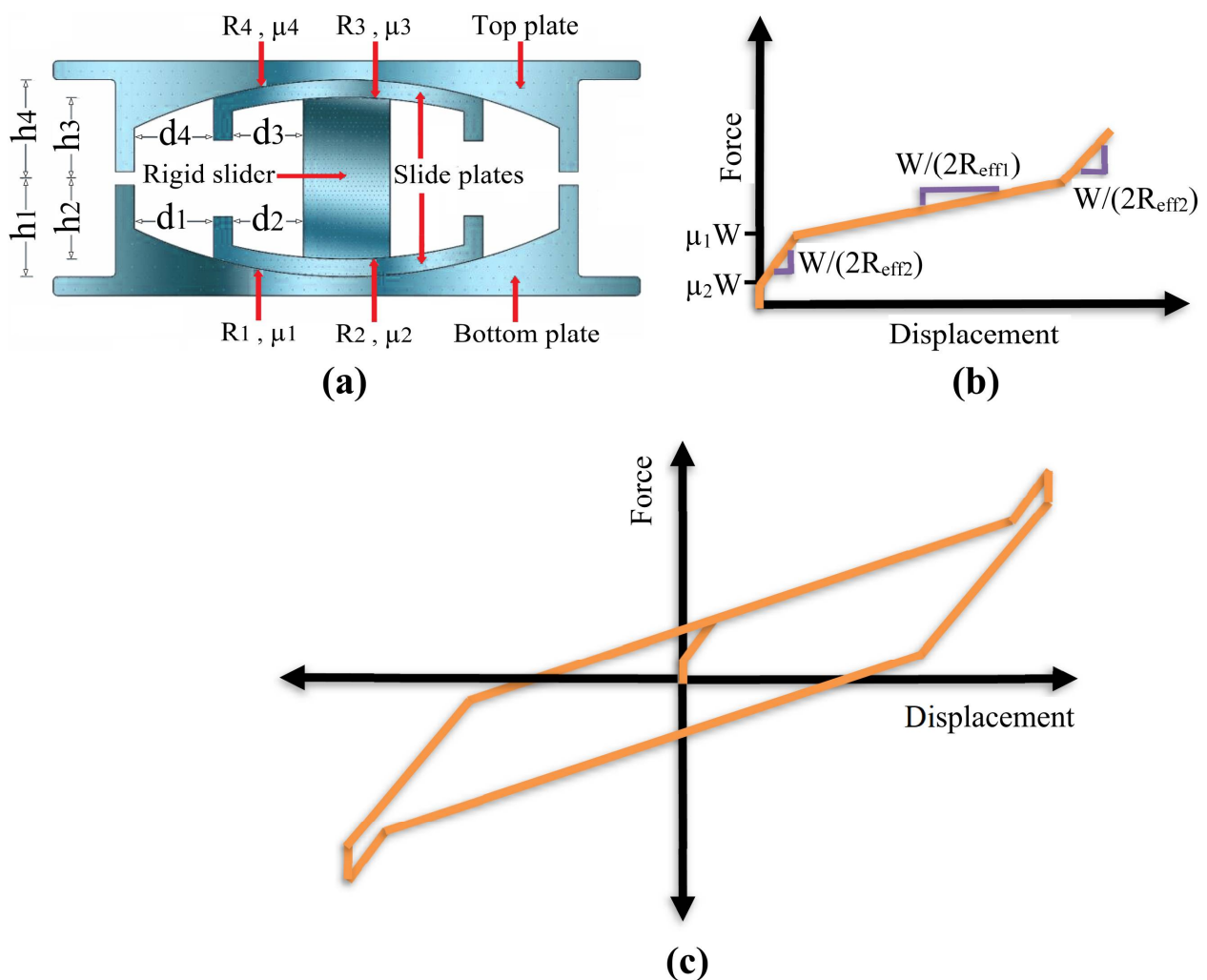


Figure 5. (a) Section of TFPI; (b) Full hysteresis loop of TFPI; (c) Force-displacement relation of the TFPI.

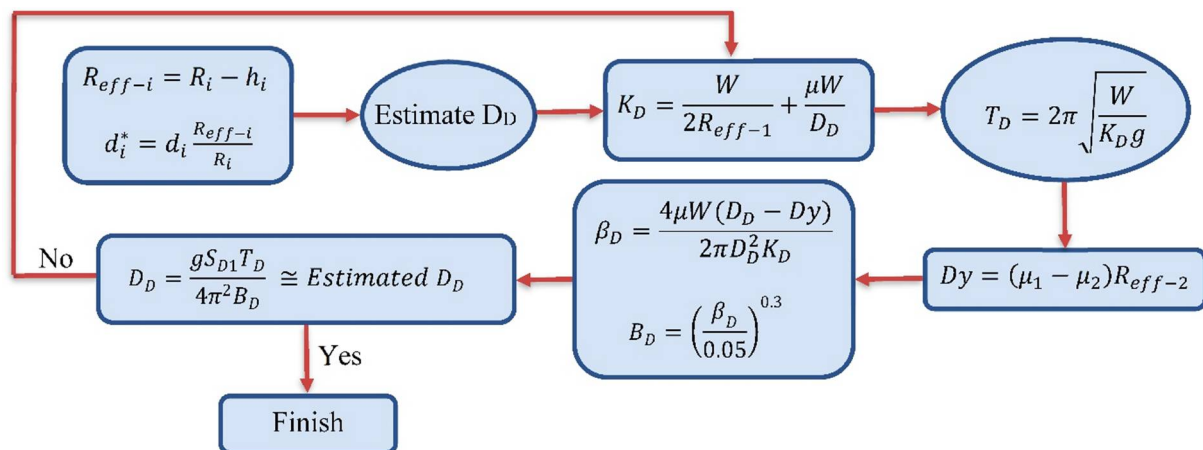


Figure 6. Design process of TFPI.

Table 2. Properties of the TFP bearings.

Frame	T_D (s)	β_D (%)	$\mu_1 = \mu_4$	$\mu_2 = \mu_3$	$R_1 = R_4$ (cm)	$R_2 = R_3$ (cm)	$d_1 = d_4$ (cm)	$d_2 = d_3$ (cm)
6	3.3	22.8	0.03	0.018	224	41	36	5
9	3.3	22.5	0.032	0.01	224	41	36	5
12	4.4	22.6	0.023	0.01	396	64	51	10

In the above flowchart, R_{eff-i} and d_i^* are the effective radius and the actual displacement capacity of the TFPI, respectively; K_D is the effective stiffness of the TFPI; W is the effective seismic weight of the structure; μ is the total equivalent friction coefficient of the TFPI; μ_1 , and μ_2 are the friction coefficients of the external and internal surfaces of the TFPI, respectively; T_D is the effective period of the TFPI; g is the gravity acceleration; D_y is the yield displacement of the TFPI; β_D and B_D are the effective damping of the TFPI and damping reduction factor, respectively.

4.2. Adding Damping and Stiffness Device (ADAS)

ADAS damper as shown in Figure 7 has been added to the stories to improve the seismic response of the structures. The results of various research [51–54] have been used to design the ADAS. According to ASCE7-10 [26], the damper is designed to be placed in both side bays of each story. Damper design steps are shown in Figure 8 and the results are shown in Table 3. S_R is calculated as the ratio of the combined horizontal stiffness of the ADAS and brace (K_a) to the story stiffness of the structure without ADAS elements (K_S). The S_R is set to 3 for 6- and 9-story structures, while it is set to 5 for a 12-story structure. The plastic (Wen) link is used to model the ADAS behavior in SAP2000 software [44]. This damper is used in stories along with chevron braces. The ratio of the lateral stiffness of the bracing member to the ADAS initial stiffness ($\frac{k_b}{k_d}$) is assumed to be 2.

In the above flowchart, $\frac{B}{D}$ is equal to $\frac{k_b}{k_d}$; E , b_1 , l , and t are the Young's modulus, the base width of ADAS plate, ADAS height, and the plate thickness, respectively; N and k_{d1} are the number of plates and the initial stiffness of each plate; V_y and F_y are the yield strength and tensile yield stress, respectively.

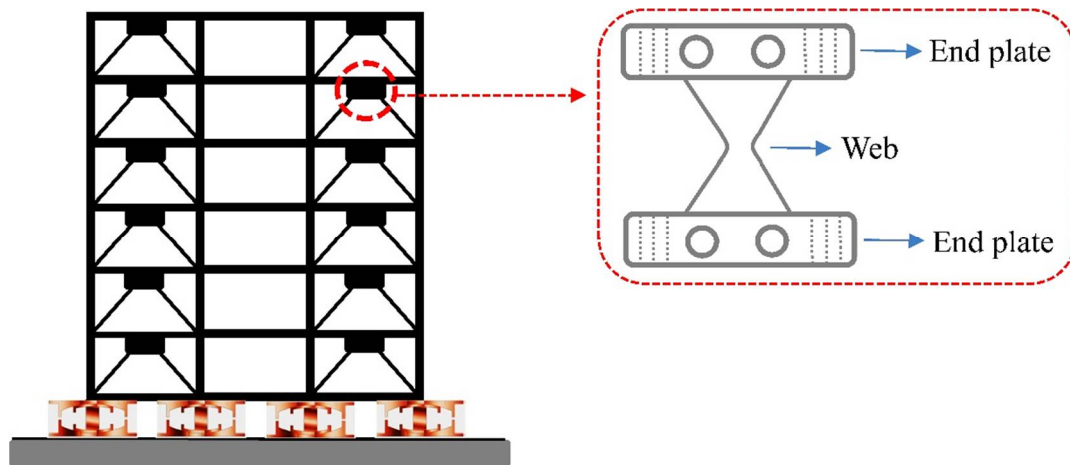


Figure 7. ADAS section and placement type in the frame.

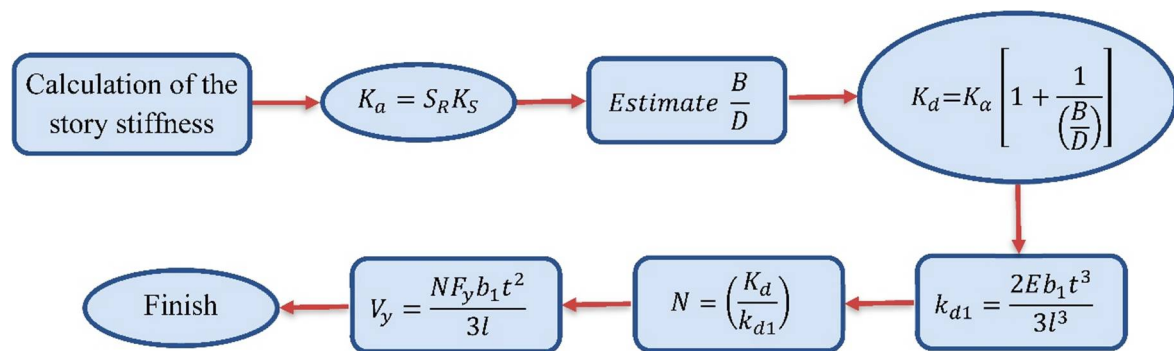


Figure 8. The design process of ADAS.

Table 3. Properties of the ADAS device.

Story		V_y (KN)		k_d (KN/mm)		
12	131			108.5		
11	175			123.2		
10	219			154		
9	219	87		154	61.6	
8	262	87		184.8	61.6	
7	700	131		208.2	92.4	
6	787	131		234.3	92.4	62.8
5	831	175	91	247.3	123.2	62.8
4	918	437	91	273.3	130.2	83.7
3	962	481	122	286.3	143.2	83.7
2	1093	525	152	325.5	156.2	104.6
1	1312	656	182	390.5	195.2	125.5

4.3. Fluid Viscous Damper (FVD)

Since it is unusual to use the ADAS damper in the isolated level, the FVD is used in the isolated level (Figure 9). The FVD force is obtained based on the damper coefficient (C), the relative velocity between the damper ends (V_C), and the damper exponent (\exp), according to Equation (1) [55]. The FVD modeling is carried out in SAP2000 software [44] based on the Maxwell model. Damper design steps are shown in Figure 10. The considered value of the damping ratio (ζ) is 15%. The value of \exp usually ranges from 0.3 to 1, which is considered 0.3 in this research. It should be noted that when $\exp = 1$, the behavior exhibits a linear, rate-dependent, hysteretic behavior, whereas for other values, the behavior is

nonlinear [56]. The value of C is calculated as 89 kN·s/m, 127.4 kN·s/m, and 122 kN·s/m for 6-, 9-, and 12-story structures, respectively.

$$F_D = C \cdot V_C^{exp} \quad (1)$$

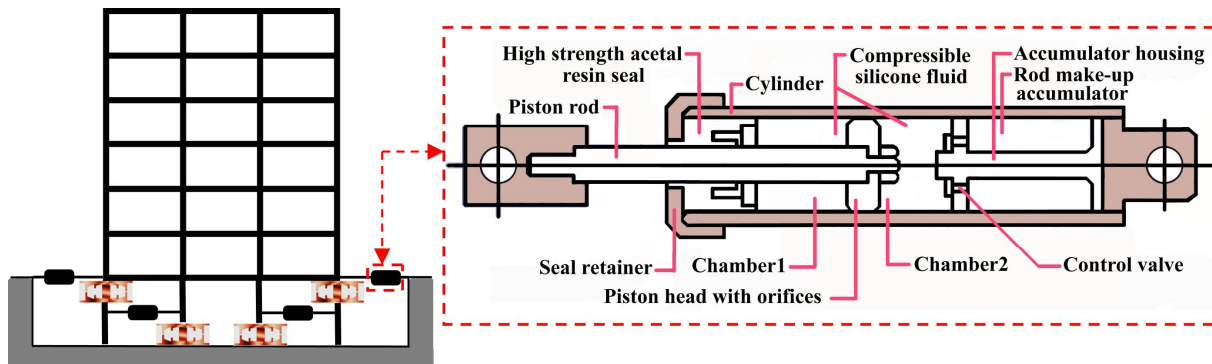


Figure 9. Installing location and cross section of the FVD.

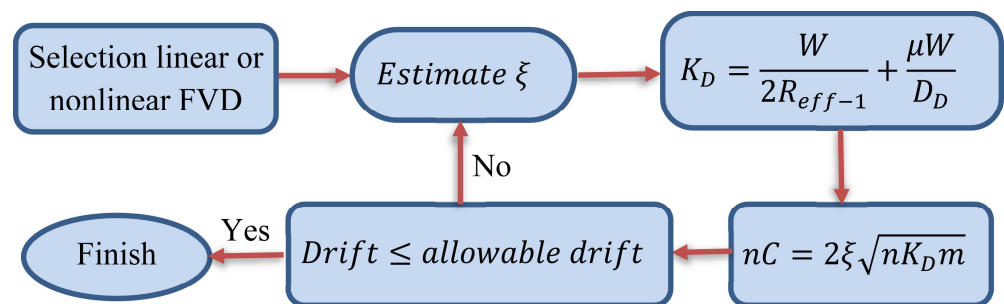


Figure 10. The design process of the FVD.

Where n and m are the total number of base TFPIs and the mass of a structure, respectively.

5. Results and Discussions

5.1. Derivation of ET Performance Curve

Endurance time excitation functions (ETEFs) exhibit a cyclical behavior, and their intensity increases over time. Consequently, the time history response of structures subjected to ETEFs displays an increasing trend, and the amplitude of the cycles also increases. The ET method enables the determination of the structure's response to various earthquake intensities. To achieve this, Equation (2) is used to obtain the maximum absolute value of the structure's response from its history in the ET method (Figure 11a,b). The absolute maximum value of the response specifies the maximum value of the response experienced up to that time.

$$\Omega(f(t)) = \text{Max}(|f(\tau)|) \quad 0 \leq \tau \leq t \quad (2)$$

where Ω is the maximum response in the time span $[0, t]$, and f is the response history as a function of time. Maximum drift, base shear, plastic rotation can be considered as response.

Due to the dynamic nature of the response, the maximum absolute value of the structures' response does not increase during each cycle. This leads to the appearance of several steps in the plot of the maximum absolute value. To remove these unwanted steps, a smoothing procedure is applied (see Figure 11c). The smoothing process is conducted using a moving average technique [32].

In the ET method, the time expresses the intensity of the earthquake. Through an analysis in the ET method, the response of a structure can be obtained in different intensities,

which is the main advantage of this method. The relationship between time and intensity is calculated in a similar way to the concept of the maximum absolute value of the response. For example, if the PGA is considered as intensity, the maximum absolute value of the acceleration at interval $[0, t]$ in the ETEF is the intensity at the time t . It should be noted that the intensity value at each time can be mapped to hazard return period (Figure 11d). This enables the ET method to obtain the response versus return period for the structure being analyzed [57].

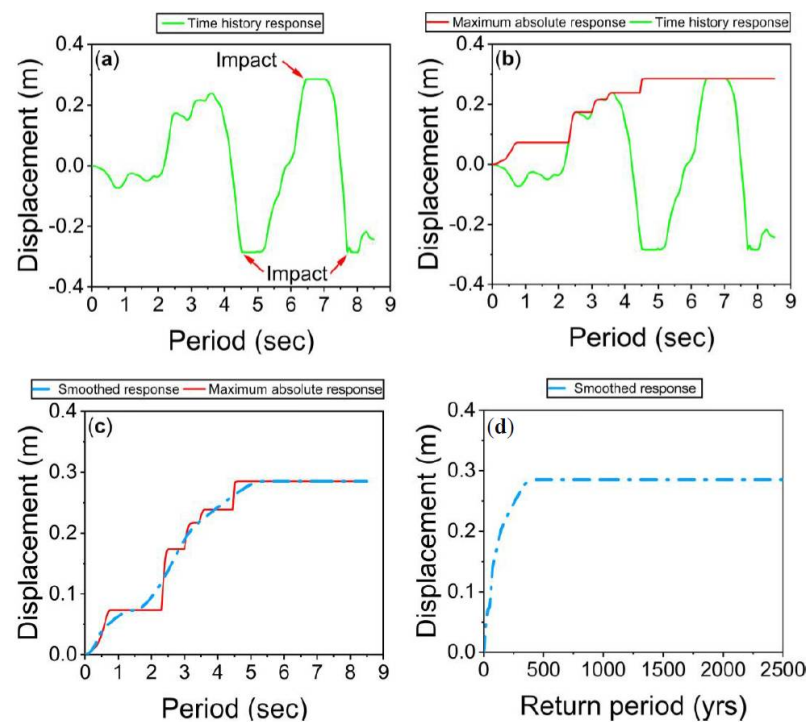


Figure 11. ET performance curve of isolated level in a 6-Story frame based on displacement under ETA40kdx01 for scenario 1: (a) Time history response, (b) Maximum absolute response, (c) Smoothed response versus time, and (d) Smoothed response versus return period.

5.2. Scenario 1

In scenario 1, the 6-, 9-, and 12-story structures have been separately modeled and analyzed by the MET method. The displacement of structures is limited at the base level by the moat wall. Figure 12 compares the inter-story drift ratio (IDR) for structures with and without dampers. According to ASCE7-16 [25], the allowable IDR is 2% for nonlinear dynamic analysis under the BSE-2 hazard level. Based on this, the 9- and 12-story structures have achieved acceptable performance, but the 6-story structure needs to be retrofitted. However, the six-story structure meets design criteria at the BSE-1 hazard level. One of the main reasons for the collapse of the six-story structure is the T_D/T_S ratio. The T_D is the same for the six- and nine-story structures, while the T_D/T_S ratio is 3 and 2.2, respectively. Therefore, the nine-story structure has experienced less IDR. This shows the importance of the superstructure flexibility when the pounding phenomenon occurs due to collision with the moat wall. As can be seen in Figure 12, the IDR of the structure with ADAS damper is better than the structure with FVD before the impact, while the results are close after the impact. It should be noted that the brace element of the ADAS damper increases the stiffness of the superstructure. Therefore, this confirms that increasing the superstructure stiffness causes the enhancement of IDR. Figure 13 shows that adding the ADAS damper to stories increases the base shear. The negative effect of adding the ADAS damper on the base shear increases significantly with the increase in the height of the structure. Consequently, the base shear of 9- and 12-story structures is about 1.5 and 2 times that of the 6-story structure under the BSE-2 hazard level, respectively. On the contrary, the addition of FVD

to the isolated level causes a decrease in base shear compared to the case without a damper. Moreover, the increase in the base shear due to the increase in the earthquake hazard level is more for the structure with ADAS than for the structure with FVD. The acceleration of isolated structures has increased greatly due to the impact (Figure 14). HAZUS 4.2 [58] has classified the failure level in acceleration-sensitive nonstructural components such as mechanical equipment into four categories. This classification is based on the intensity of acceleration, which includes $0.3\text{ g} \leq \text{slight} < 0.6\text{ g}$, $0.6\text{ g} \leq \text{moderate} < 1.2\text{ g}$, $1.2\text{ g} \leq \text{extensive} < 2.4\text{ g}$, and $2.4\text{ g} \leq \text{complete}$. The acceleration-sensitive nonstructural components of the structures without supplementary damper are in a complete collapse state due to the abrupt increase in acceleration after impact. Adding the ADAS damper has an insignificant effect on reducing the acceleration of 6- and 9-story structures. Additionally, the ADAS damper increases the acceleration of the 12-story structure. On the other hand, considering FVD in the isolated level is ineffective on the stiffness of the superstructure. Therefore, FVD has been able to significantly reduce acceleration. However, the acceleration-sensitive nonstructural components are still in the complete collapse state. Indeed, improving the performance of structural elements during the pounding has not improved the performance of acceleration-sensitive nonstructural components.

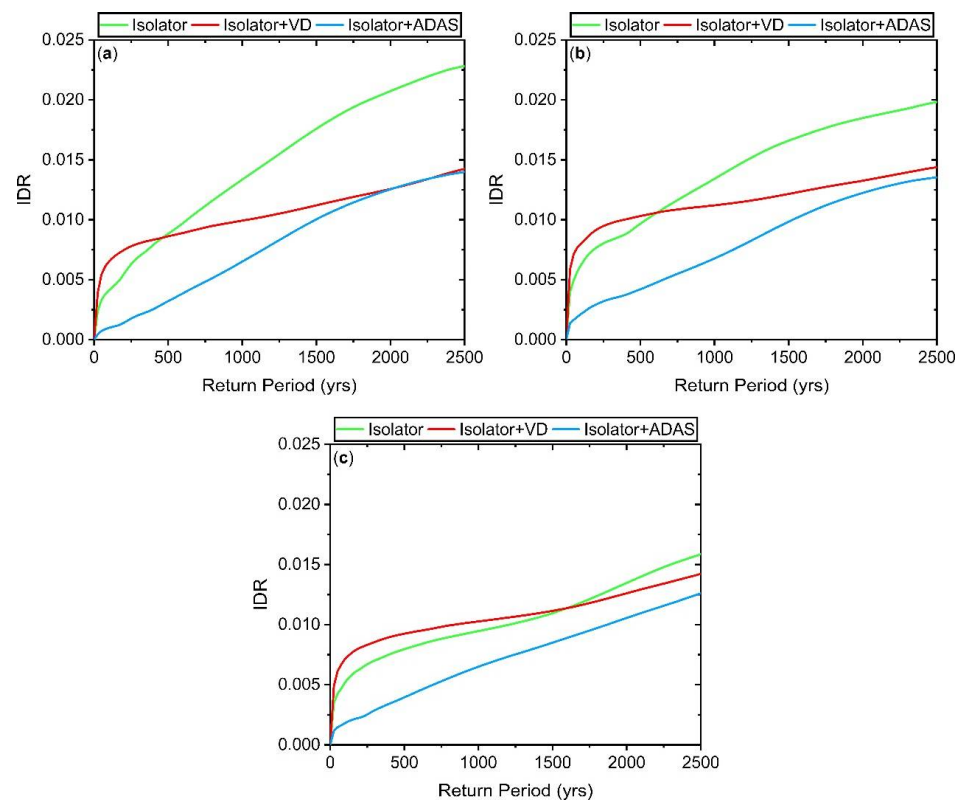


Figure 12. ET performance curve based on the maximum IDR for scenario 1: (a) 6-story isolated structure; (b) 9-story isolated structure; (c) 12-story isolated structure.

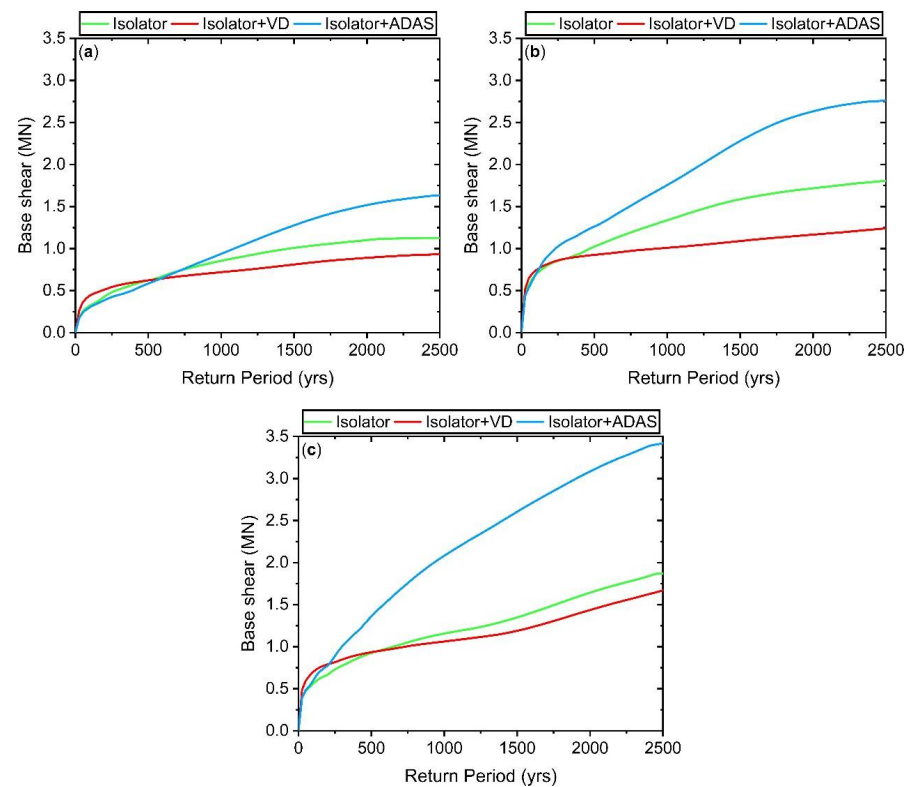


Figure 13. ET performance curve based on the base shear for scenario 1: (a) 6-story isolated structure; (b) 9-story isolated structure; (c) 12-story isolated structure.

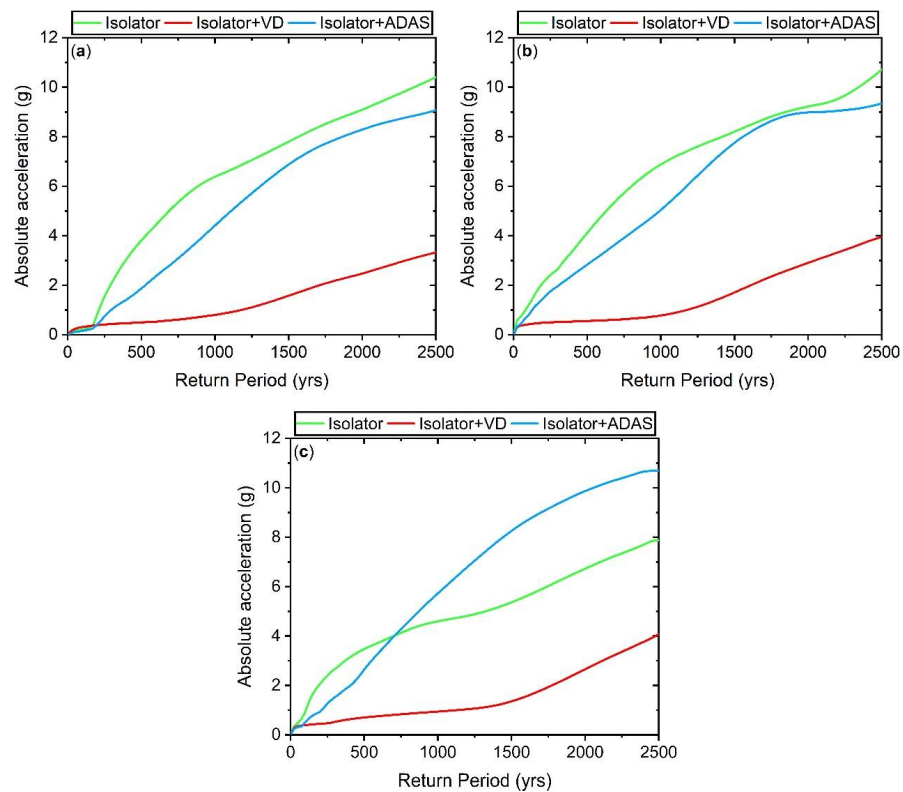


Figure 14. ET performance curve based on the maximum absolute acceleration for scenario 1: (a) 6-story isolated structure; (b) 9-story isolated structure; (c) 12-story isolated structure.

5.3. Scenario 2

In scenario 2, the 6, 9, and 12-story structures are placed next to each other so that the 9-story structure is placed between 2 other structures. Additionally, displacement of the isolators is limited by the moat wall. The performance of structures based on the IDR is shown in Figure 15 by the ET curve. The results show that the maximum IDR of all three isolated structures has increased under the BSE-2 hazard level as compared to Scenario 1. However, this increase is less for the 12-story structure. The nine-story structure, which is located between two other structures, has experienced the highest IDR. This matter shows that the taller isolated structure increases the damage of the shorter isolated structure. The results of the six-story structure, which is limited by the nine-story structure and the moat wall, also confirm this matter. In the first step of retrofitting, dampers have been added to the 6- and 9-story structures, which failed under the BSE-2 hazard level according to ASCE7-16 [25]. In the next step, dampers were added to all three structures. Adding the ADAS damper to the failed structures could not improve the behavior of the structure under most of the earthquake hazard levels. The negative effect of the ADAS damper significantly increases by increasing the height of the structure. The addition of ADAS to all three structures decreases IDR as compared to adding ADAS only to the failed structures. However, the structure's performance is still unacceptable under the BSE-2 hazard level. The ADAS damper is added to the stories along with the braces, which has increased the stiffness of the structures; this increases the severity of the impact between structures and hence reduces the efficiency of the ADAS damper. Adding FVD to failed structures reduces the IDR of 6- and 9-story structures after the impact. Nevertheless, adding FVD to all three structures did not significantly change the IDR in the six- and nine-story structures as compared to adding FVD to failed structures. The behavior of the 12-story structure with the addition of FVD is different from the behavior of the 6- and 9-story structures. Adding FVD to failed structures increases the IDR under the BSE-2 hazard level, but adding FVD to all three structures reduces the IDR. This shows that the impact intensity of the 12-story structure has increased if only the damping of the shorter isolated structure (9 stories) increases.

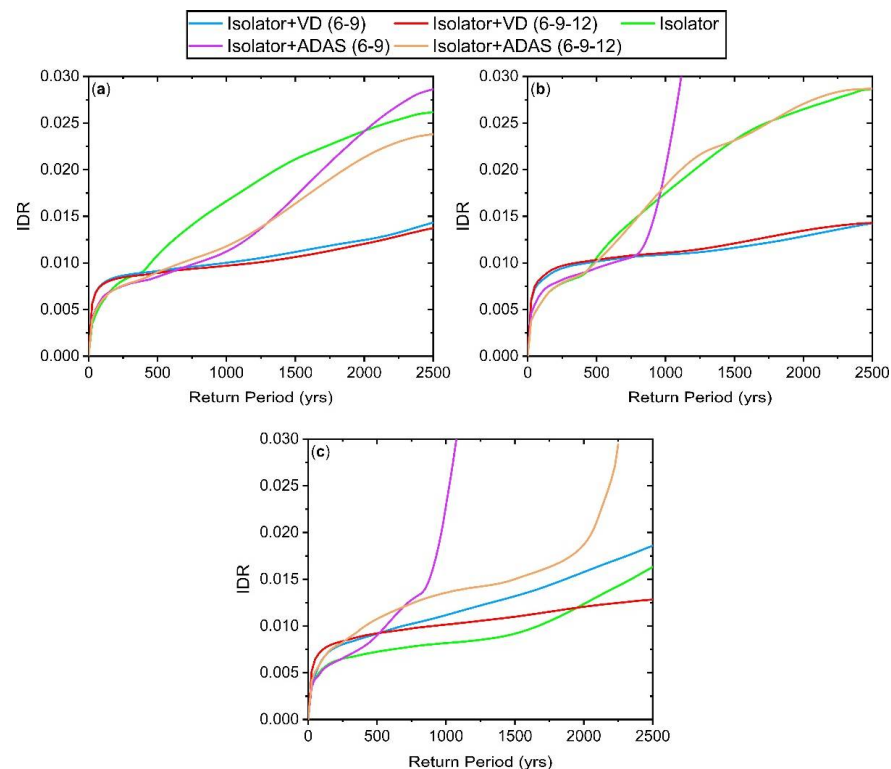


Figure 15. ET performance curve based on the maximum IDR for scenario 2: (a) 6-story isolated structure; (b) 9-story isolated structure; (c) 12-story isolated structure.

Figure 16 compares the absolute acceleration of structures with and without dampers. The absolute acceleration of 6- and 9-story structures has become more critical by placing structures next to each other as compared to scenario 1. However, the acceleration of the 12-story structure has not significantly changed, which could be due to more displacement capacity in this structure. According to the HAZUS 4.2 [58], adding ADAS and FVD dampers could not reduce the damage of acceleration-sensitive nonstructural components under the BSE-2 hazard level. However, the performance of the FVD at the isolated level is much better than ADAS in stories. Adding the ADAS to all three structures as compared to adding it only to the failed structures has decreased the acceleration in six- and nine-story structures, but this has increased acceleration in the 12-story structure. The reverse situation is observed for FVD. It seems that when isolated structures are placed next to each other, using additional damping on the isolated level to reduce absolute acceleration is more effective in the structure with a large displacement capacity. The impact force of the isolated structure on the adjacent structure increases with the enhancement of its displacement capacity, so its acceleration also increases.

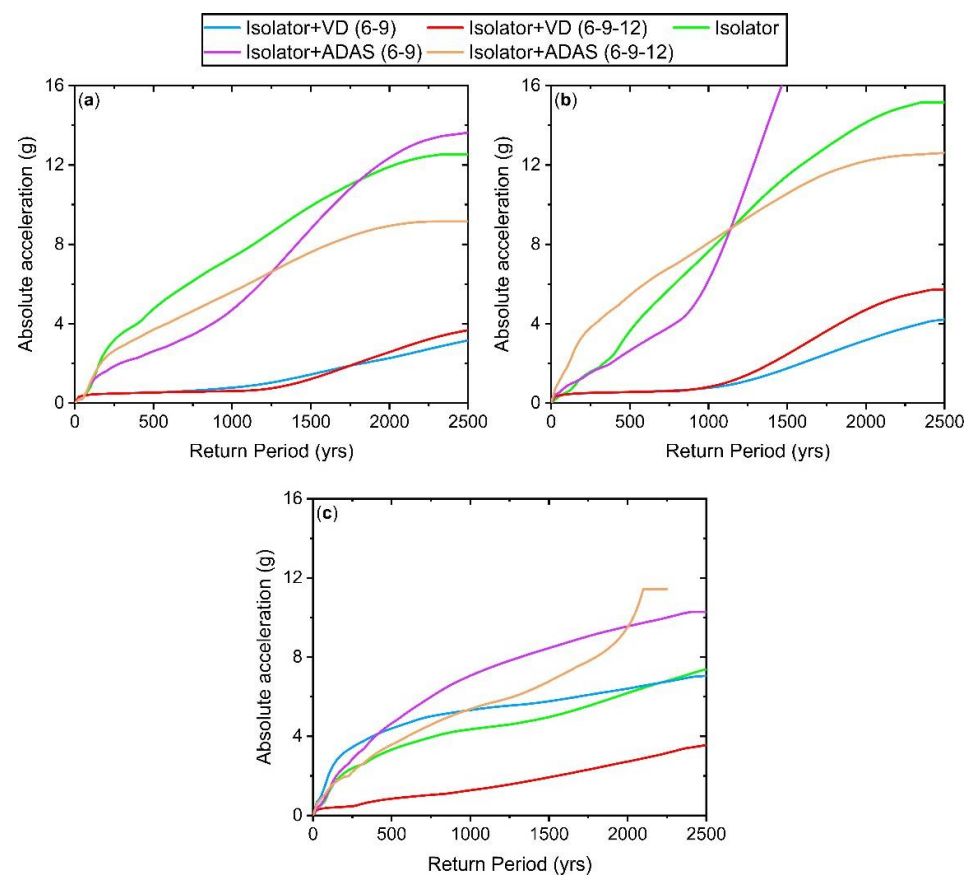


Figure 16. ET performance curve based on the maximum absolute acceleration for scenario 2: (a) 6-story isolated structure; (b) 9-story isolated structure; (c) 12-story isolated structure.

5.4. Scenario 3

In scenario 3, the 12-story structure is located in the middle of other structures. The ET curve of structures based on IDR is shown in Figure 17. The results show that the 6- and 9-story structures have an unacceptable performance under the BSE-2 hazard level. Their IDR has also increased as compared to Scenario 1. The 12-story structure has experienced the minimum IDR. The reason for this could be the greater displacement capacity of the 12-story structure as compared to other structures. As in Scenario 2, the ADAS and FVD dampers are first added to the failed structures and then added to all structures. The results show that unlike scenario 2, adding ADAS to the failed structures leads to better results

in them. However, in the 12-story structure, a similar performance to Scenario 2 can be seen by adding ADAS. As a result, if two isolated structures are located next to each other, adding ADAS to the shorter isolated structure decreases IDR in the shorter structure, while increasing IDR in the taller structure. The influence of FVD when added to the isolated level is similar to Scenario 2 in all three structures.

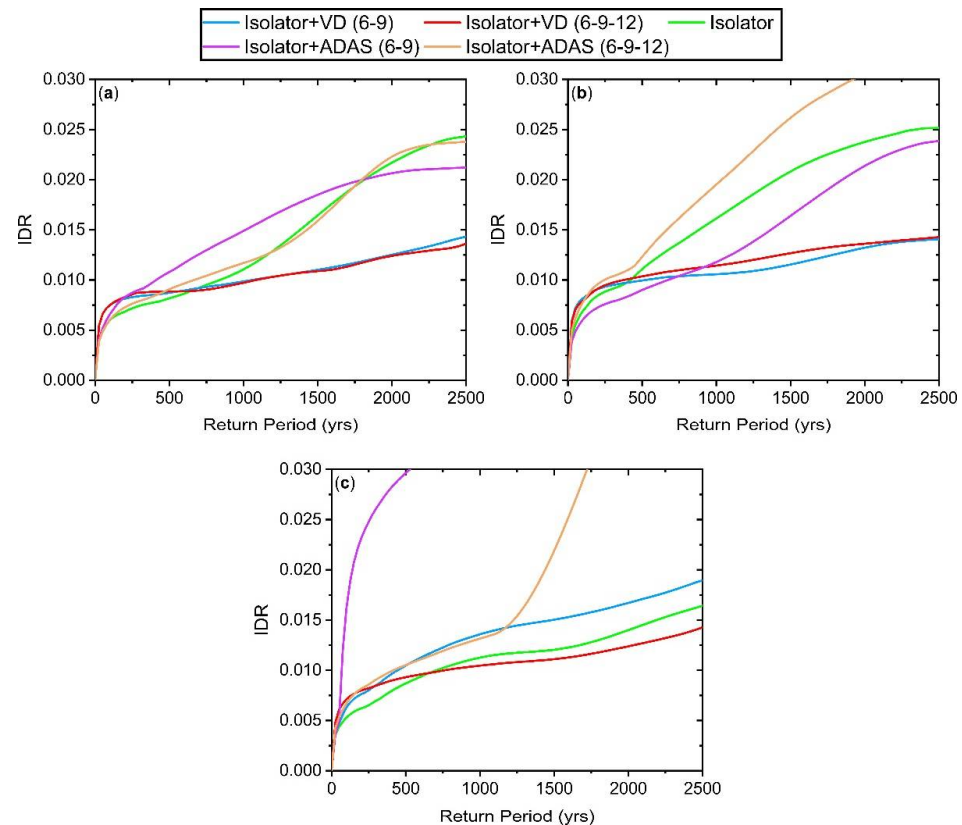


Figure 17. ET performance curve based on the maximum IDR for scenario 3: (a) 6-story isolated structure; (b) 9-story isolated structure; (c) 12-story isolated structure.

The acceleration-sensitive nonstructural components before and after adding the ADAS or FVD under the BSE-2 hazard level are in the complete collapse state (Figure 18). Unlike scenario 2, adding ADAS to all three structures shows more acceleration than adding ADAS to failed structures under the BSE-2 hazard level. Adding the FVD to all three structures has improved the performance of 9- and 12-story structures as compared to adding it only to failed structures. Similar to scenario 2, adding the FVD to the 12-story structure that has a higher displacement capacity than other structures is more effective. It seems that at the moment when the impact occurred, we should witness a noticeable change in the slope of response curves. However, the drawn curves are completely smooth. This is because of the smoothing process in the ET method.

5.5. Scenario 4

In scenario 4, the 9- and 12-story structures are located on both sides of the 6-story structure. The results shown in Figure 19 indicate that the condition of the 9- and 12-story structures is more critical compared to other scenarios. The comparison of the Scenario 4 condition with other scenarios shows that the IDR of adjacent structures can become more critical if the middle structure is shorter than the exterior structures. It is observed in scenarios 2 and 3 that the presence of a taller isolated structure in the adjacency of the isolated structure does not reduce the IDR of the shorter isolated structure. Similar to scenario 1, the taller structure has not decreased the IDR of the 6-story structure. The IDR of all three structures has exceeded the permissible IDR of ASCE7-16 [25] under the BSE-2

hazard level and they need to be retrofitted. Adding FVD to all three structures at the isolated level reduced their IDR to the allowable limit. However, adding the ADAS damper on all floors was effective only for the 9-story structure to make the IDR response lie within the permissible limit.

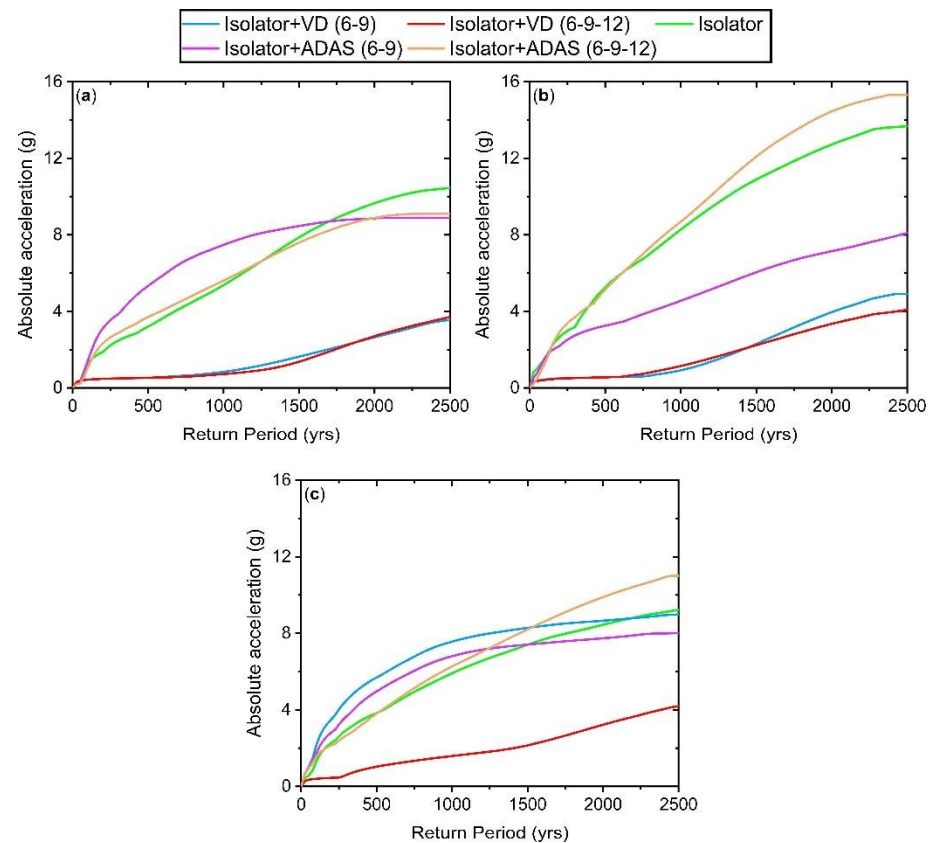


Figure 18. ET performance curve based on the maximum absolute acceleration for scenario 3: (a) 6-story isolated structure; (b) 9-story isolated structure; (c) 12-story isolated structure.

Figure 20 shows that acceleration-sensitive nonstructural components are in the state of complete collapse under the BSE-2 hazard level according to the HAZUS 4.2 [58]. Similar to the previous scenarios, structures experience very high acceleration under impact. Komodromos et al. [7] obtained the maximum acceleration of a five-story isolated structure up to 140 m/s^2 under impact. Moreover, Masroor and Mosqueda [8] found a maximum acceleration of more than 7 g for a three-story isolated structure under impact. According to the mentioned studies, an acceleration of more than 2.4 g is normal for isolated structures with displacement capacity equal to the requirement displacement capacity for the BSE-1 hazard level, while the building is under the BSE-2 hazard level intensity. Adding ADAS damper has also increased acceleration, while FVD has significantly reduced acceleration. However, more damping for FVD is needed to achieve better performance of acceleration-sensitive nonstructural components.

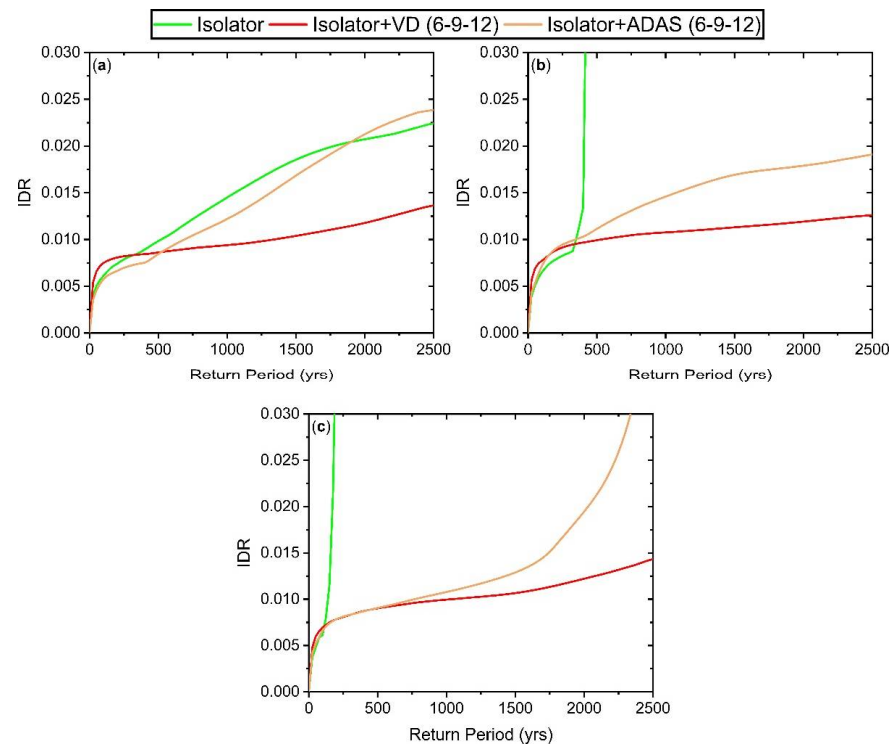


Figure 19. ET performance curve based on the maximum IDR for scenario 4: (a) 6-story isolated structure; (b) 9-story isolated structure; (c) 12-story isolated structure.

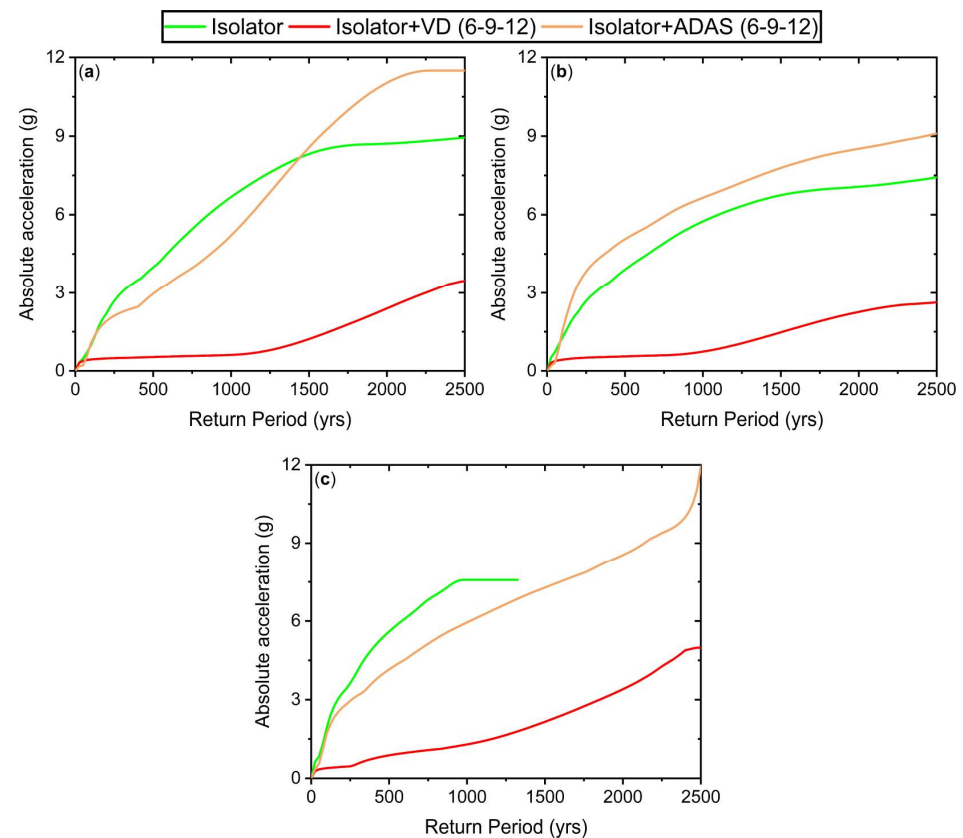


Figure 20. ET performance curve based on the maximum absolute acceleration for scenario 4: (a) 6-story isolated structure; (b) 9-story isolated structure; (c) 12-story isolated structure.

6. Summary and Conclusions

In this study, the performance of isolated structures was studied by considering impact during earthquakes with intensities higher than the considered intensity in the design step. For this purpose, 3 isolated frames (6, 9, and 12 stories) with the IMF system were designed under the BSE-1 hazard level. The displacement capacity of isolated structures was limited by the moat wall and the adjacent isolated structure. The structures were evaluated in four different scenarios by MET analysis under variable earthquake hazard levels. The effect of ADAS damper on stories and FVD at the isolated level was also investigated to improve the performance of the structures. The obtained results are as follows:

- There is a high collapse probability for the isolated structure with displacement capacity according to the BSE-1 hazard level under the BSE-2 hazard level. This is because of the pounding phenomena.
- The damage intensity of isolated structures due to impact with the adjacent isolated structure is higher than the impact with the moat wall.
- Decreasing the T_D/T_S can enhance the performance of isolated structural components under impact with the moat wall.
- Using the damper in the stories instead of the isolated level is more effective (about 1.62–11.6% under the BSE-2 hazard level) for improving the performance of the structural components under the impact with the moat wall. In contrast, using the damper at the isolated level is more effective (about 51.35–537% under the BSE-2 hazard level) for the impact of the adjacent isolated structures.
- The taller isolated structure can increase the failure of structural components of the adjacent shorter isolated structure under the impact between them.
- Adding the damper only to the shorter structure at the isolated level or in the stories increases the damage of the taller isolated structure under the impact between them, but adding the damper to both structures improves the performance of the structural components.
- Adding the damper to the isolated level is more effective than adding the damper to the stories (about 46–408% under the BSE-2 hazard level) in most scenarios for reducing the damage of the acceleration-sensitive nonstructural components under both types of impact mechanisms. Moreover, the positive effect of adding the damper to the isolated level was increased by enhancing the displacement capacity of the isolator in case of impact with the adjacent isolated structures.

Author Contributions: Conceptualization, A.M., A.S.-M., M.M., S.Z. and O.B.; methodology, A.M., A.S.-M., M.M., S.Z. and O.B.; software, A.M. and A.S.-M.; validation, D.D.D.; investigation, M.M., S.Z., O.B. and D.D.D.; writing—original draft preparation, A.M. and A.S.-M.; writing—review and editing, M.M., S.Z., O.B. and D.D.D.; supervision, D.D.D. All authors have read and agreed to the published version of the manuscript.

Funding: This research received no external funding.

Data Availability Statement: The data used to support the findings of this study are included within the article.

Conflicts of Interest: The authors declare that they have no conflict of interest.

References

1. Pourmasoud, M.M.; Lim, J.B.P.; Hajirasouliha, I.; McCrum, D. Multi-directional base isolation system for coupled horizontal and vertical seismic excitations. *J. Earthq. Eng.* **2022**, *26*, 1145–1170. [[CrossRef](#)]
2. Rakicevic, Z.; Bogdanovic, A.; Farsangi, E.N.; Sivandi-Pour, A. A hybrid seismic isolation system toward more resilient structures: Shaking table experiment and fragility analysis. *J. Build. Eng.* **2021**, *38*, 102194. [[CrossRef](#)]
3. Farsangi, E.N.; Tasnimi, A.A.; Yang, T.; Takewaki, I.; Mohammadhasani, M. Seismic performance of base-isolated buildings under multi-directional earthquake excitations. *Smart Struct. Syst.* **2018**, *22*, 383–397.
4. Vibhute, A.S.; Bharti, S.D.; Shrimali, M.K.; Datta, T.K. Performance evaluation of FPS and LRB isolated frames under main and aftershocks of an earthquake. *Structures* **2022**, *44*, 1532–1545. [[CrossRef](#)]

5. Özüygür, A.R.; Farsangi, E.N. Influence of pulse-pike near-fault ground motions on the base-isolated buildings with LRB devices. *Pract. Period. Struct. Des. Constr.* **2021**, *26*, 04021027. [\[CrossRef\]](#)
6. Asadi, P.; Nikfar, D.; Hajirasouliha, I. Life-cycle cost based design of bridge lead-rubber isolators in seismic regions. *Structures* **2020**, *27*, 383–395. [\[CrossRef\]](#)
7. Komodromos, P.; Polycarpou, P.C.; Papaloizou, L.; Phocas, M.C. Response of seismically isolated buildings considering poundings. *Earthq. Eng. Struct. Dyn.* **2007**, *36*, 1605–1622. [\[CrossRef\]](#)
8. Masroor, A.; Mosqueda, G. Experimental simulation of base-isolated buildings pounding against moat wall and effects on superstructure response. *Earthq. Eng. Struct. Dyn.* **2012**, *41*, 2093–2109. [\[CrossRef\]](#)
9. Masroor, A.; Mosqueda, G. Assessing the Collapse Probability of Base-Isolated Buildings considering Pounding to Moat Walls using the FEMA P695 Methodology. *Earthq. Spectra* **2015**, *31*, 2069–2086. [\[CrossRef\]](#)
10. ASCE/SEI 7-05; Minimum Design Loads for Buildings and Other Structures. American Society of Civil Engineers: Reston, VA, USA, 2006.
11. Matsagar, V.A.; Jangid, R. Seismic response of base-isolated structures during impact with adjacent structures during impact with adjacent structures. *Eng. Struct.* **2003**, *25*, 1311–1323. [\[CrossRef\]](#)
12. Pant, D.R.; Wijeyewickrema, A.C. Structural performance of a base-isolated reinforced concrete building subjected to seismic pounding. *Earthq. Eng. Struct. Dyn.* **2012**, *41*, 1709–1716. [\[CrossRef\]](#)
13. Bao, Y.; Becker, T.C. Effect of design methodology on collapse of friction pendulum isolated moment-resisting and concentrically braced frames. *J. Struct. Eng.* **2018**, *144*, 04018203. [\[CrossRef\]](#)
14. Bao, Y.; Becker, T.C. Inelastic response of base-isolated structures subjected to impact. *Eng. Struct.* **2018**, *171*, 86–93. [\[CrossRef\]](#)
15. Movahhed, A.S.; Zardari, S.; Şadoğlu, E. Seismic performance of a building base-isolated by TFP susceptible to pound with a surrounding moat wall. *Earthq. Struct.* **2022**, *23*, 723–736.
16. Rayegani, A.; Nouri, G. Seismic collapse probability and life cycle cost assessment of isolated structures subjected to pounding with smart hybrid isolation system using a modified fuzzy based controller. *Structures* **2022**, *44*, 30–41. [\[CrossRef\]](#)
17. Rawlinson, T.A.; Marshall, J.D.; Ryan, K.L.; Zargar, H. Development and experimental evaluation of a passive gap damper device to prevent pounding in base-isolated structures. *Earthq. Eng. Struct. Dyn.* **2015**, *44*, 1661–1675. [\[CrossRef\]](#)
18. Zargar, H.; Ryan, K.L.; Marshall, J.D. Feasibility study of a gap damper to control seismic isolator displacements in extreme earthquakes. *Struct. Control Health Monit.* **2013**, *20*, 1159–1175. [\[CrossRef\]](#)
19. Zargar, H.; Ryan, K.L.; Rawlinson, T.A.; Marshall, J.D. Evaluation of a passive gap damper to control displacements in a shaking test of a seismically isolated three-story frame. *Earthq. Eng. Struct. Dyn.* **2017**, *46*, 51–71. [\[CrossRef\]](#)
20. Matsagar, V.A.; Jangid, R.S. Viscoelastic damper connected to adjacent structures involving seismic isolation. *J. Civ. Eng. Manag.* **2005**, *11*, 309–322. [\[CrossRef\]](#)
21. Shrimali, M.; Bharti, S.; Dumne, S. Seismic response analysis of coupled building involving MR damper and elastomeric base isolation. *Ain Shams Eng. J.* **2015**, *6*, 457–470. [\[CrossRef\]](#)
22. Khatami, S.M.; Naderpour, H.; Mortezaei, A.; Sharbatdar, A.; Lasowicz, N.; Jankowski, R. The Effectiveness of Rubber Bumpers in Reducing the Effects of Earthquake-Induced Pounding between Base-Isolated Buildings. *Appl. Sci.* **2022**, *12*, 4971. [\[CrossRef\]](#)
23. Zhou, Y.; Chen, P. Shaking table tests and numerical studies on the effect of viscous dampers on an isolated RC building by friction pendulum bearings. *Soil Dyn. Earthq. Eng.* **2017**, *100*, 330–344. [\[CrossRef\]](#)
24. Chen, P.; Wu, X. Investigations on the Dynamic Response of Adjacent Buildings Connected by Viscous Dampers. *Buildings* **2022**, *12*, 1480. [\[CrossRef\]](#)
25. ASCE/SEI 7-16; Minimum Design Loads and Associated Criteria for Buildings and Other Structures. American Society of Civil Engineers: Reston, VA, USA, 2017.
26. ASCE/SEI 7-10; Minimum Design Loads for Buildings and Other Structures. American Society of Civil Engineers: Reston, VA, USA, 2010.
27. Kitayama, S.; Constantinou, M.C. Collapse performance of seismically isolated buildings designed by the procedures of ASCE/SEI 7. *Eng. Struct.* **2018**, *164*, 243–258. [\[CrossRef\]](#)
28. Beheshti, M.; Asadi, P. Lifetime performance assessment of ductile steel frame using fractional model of viscoelastic dampers considering uncertainty parameters. *Mech. Based Des. Struct. Mach.* **2022**, *50*, 3157–3179. [\[CrossRef\]](#)
29. Asadpour, G.; Asadi, P.; Hajirasouliha, I. Analysis of bilinear hysteretic structures with nonlinear fluid viscous dampers using modified stochastic linearization technique. *Eng. Struct.* **2022**, *251*, 113555. [\[CrossRef\]](#)
30. Estekanchi, H.; Vafai, A.; Sadeghazar, M. Endurance time method for seismic analysis and design of structures. *Sci. Iran.* **2004**, *11*, 341–370.
31. Tavakolinia, M.; Basim, M.C. Performance-based optimum tuning of tuned mass dampers on steel moment frames for seismic applications using the endurance time method. *Earthq. Eng. Struct. Dyn.* **2021**, *50*, 3646–3669. [\[CrossRef\]](#)
32. Estekanchi, H.; Riahi, H.; Vafai, A. Application of endurance time method in seismic assessment of steel frames. *Eng. Struct.* **2011**, *33*, 2535–2546. [\[CrossRef\]](#)
33. Nozari, A.; Estekanchi, H. Optimization of endurance time acceleration functions for seismic assessment of structures. *Int. J. Optim. Civ. Eng.* **2011**, *1*, 257–277.
34. Mashayekhi, M.; Estekanchi, H. Significance of Effective Number of Cycles in Endurance Time Analysis. *Asian J. Civ. Eng. (Build. Hous.)* **2012**, *13*, 647–657.

35. Mashayekhi, M.; Estekanchi, H.E. Investigation of Strong-Motion Duration Consistency in Endurance Time Excitation Functions. *Sci. Iran.* **2013**, *20*, 1085–1093.
36. Mashayekhi, M.; Estekanchi, H.E.; Vafai, A.; Mirfarhadi, S.A. Simulation of cumulative absolute velocity consistent endurance time excitations. *J. Earthq. Eng.* **2021**, *25*, 892–917. [[CrossRef](#)]
37. Vaiana, N.; Capuano, R.; Rosati, L. Evaluation of path-dependent work and internal energy change for hysteretic mechanical systems. *Mech. Syst. Signal Process.* **2023**, *186*, 109862. [[CrossRef](#)]
38. Mashayekhi, M.; Estekanchi, H.E.; Vafai, H.; Mirfarhadi, S.A. Development of hysteretic energy compatible endurance time excitations and its application. *Eng. Struct.* **2018**, *177*, 753–769. [[CrossRef](#)]
39. FEMA P-695; Quantification of Building Seismic Performance Factors. FEMA: Washington, DC, USA, 2009.
40. Movahhed, A.S.; Shirkhani, A.; Zardari, S.; Mashayekhi, M.; Farsangi, E.N.; Majdi, A. Modified endurance time method for seismic performance assessment of base-isolated structures. *J. Build. Eng.* **2023**, *67*, 105955. [[CrossRef](#)]
41. ANSI/AISC 360-16; Specification for Structural Steel Buildings. American Institute of Steel Construction: Chicago, IL, USA, 2016.
42. ANSI/AISC 341-16; Seismic Provisions for Structural Steel Buildings. American Institute of Steel Construction: Chicago, IL, USA, 2016.
43. ASCE/SEI 41-17; Seismic Evaluation and Retrofit of Existing Buildings. American Society of Civil Engineers: Reston, VA, USA, 2017.
44. SAP2000; Integrated Solution for Structural Analysis and Design. Computers and Structures Inc.: Berkeley, CA, USA, 2009.
45. Movahhed, A.S.; Shirkhani, A.; Zardari, S.; Farsangi, E.N.; Pour, A.K. Effective range of base isolation design parameters to improve structural performance under far and near-fault earthquakes. *Adv. Struct. Eng.* **2023**, *26*, 52–71. [[CrossRef](#)]
46. Hughes, P.J.; Mosqueda, G. Evaluation of uniaxial contact models for moat wall pounding simulations. *Earthq. Eng. Struct. Dyn.* **2020**, *49*, 1197–1215. [[CrossRef](#)]
47. Fenz, D.M.; Constantinou, M.C. Spherical sliding isolation bearings with adaptive behavior: Theory. *Earthq. Eng. Struct. Dyn.* **2008**, *37*, 163–183. [[CrossRef](#)]
48. Fenz, D.M.; Constantinou, M.C. Spherical sliding isolation bearings with adaptive behavior: Experimental verification. *Earthq. Eng. Struct. Dyn.* **2008**, *37*, 185–205. [[CrossRef](#)]
49. Fenz, D.M.; Constantinou, M.C. Modeling triple friction pendulum bearings for response-history analysis. *Earthq. Spectra* **2008**, *24*, 1011–1028. [[CrossRef](#)]
50. Constantinou, M.; Kalpakidis, I.; Filiatrault, A.; Lay, R.E. *LRFD-Based Analysis and Design Procedures for Bridge Bearings and Seismic Isolators*; Technical Report No. MCEER-11-0004; State University of New York at Buffalo: Buffalo, NY, USA, 2011.
51. Xia, C.; Hanson, R.D. Influence of ADAS element parameters on building seismic response. *J. Struct. Eng.* **1992**, *118*, 1903–1918. [[CrossRef](#)]
52. Tehranizadeh, M. Passive energy dissipation device for typical steel frame building in Iran. *Eng. Struct.* **2001**, *21*, 643–655. [[CrossRef](#)]
53. Bayat, M.; Abdollahzade, G. Analysis of the steel braced frames equipped with ADAS devices under the far field records. *Lat. Am. J. Solids Struct.* **2011**, *8*, 163–181. [[CrossRef](#)]
54. Whittaker, A.S.; Bertero, V.V.; Alonso, L.J.; Thompson, C.L. *Earthquake Simulator Testing of Steel Plate Added Damping and Stiffness Elements*; Report No. UCB/EERC-89/02; Earthquake Engineering Research Center, University of California: Berkeley, CA, USA, 1989.
55. Providakis, C. Effect of supplemental damping on LRB and FPS seismic isolators under near-fault ground motions. *Soil Dyn. Earthq. Eng.* **2009**, *29*, 80–90. [[CrossRef](#)]
56. Vaiana, N.; Sessa, S.; Marmo, F.; Rosati, L. Nonlinear dynamic analysis of hysteretic mechanical systems by combining a novel rate-independent model and an explicit time integration method. *Nonlinear Dyn.* **2019**, *98*, 2879–2901. [[CrossRef](#)]
57. Mirzaee, A.; Estekanchi, H.; Vafai, A. Improved methodology for endurance time analysis: From time to seismic hazard return period. *Sci. Iran.* **2012**, *19*, 1180–1187. [[CrossRef](#)]
58. Hazus 4.2; Hazus Earthquake Model Technical Manual. Federal Emergency Management Agency: Washington, DC, USA, 2020.

Disclaimer/Publisher's Note: The statements, opinions and data contained in all publications are solely those of the individual author(s) and contributor(s) and not of MDPI and/or the editor(s). MDPI and/or the editor(s) disclaim responsibility for any injury to people or property resulting from any ideas, methods, instructions or products referred to in the content.